Postprint of: Wójcik N., Tagiara N., Ali S., Górnicka K., Segawa H., Klimczuk T., Jonson B., Möncke D., Kamitsos E.: Structure and magnetic properties of $BeO-Fe_2O_3-Al_2O_3-TeO_2$ glass-ceramic composites, JOURNAL OF THE EUROPEAN CERAMIC SOCIETY (2021), https://doi.org/10.1016/j.jeurceramsoc.2021.04.005

Structure and magnetic properties of $BeO-Fe_2O_3-Al_2O_3-TeO_2$ glass-ceramic composites

N. A. Wójcik[1,2*], N. S. Tagiara[3], S. Ali[2], K. Górnicka[1], H. Segawa[2,5], T. Klimczuk[1], B. Jonson[2], D. Möncke[2,3,4], E. I. Kamitsos[3]

[1]*Department of Solid State Physics, Faculty of Applied Physics and Mathematics, Gdańsk University of Technology, Narutowicza Street 11/12, 80–233 Gdańsk, Poland*

[2]*Department of Built Environment and Energy Technology, Linnæus University, 35195 Växjö, Sweden*

[3]*Theoretical and Physical Chemistry Institute, National Hellenic Research Foundation, 48 Vassileos Constantinou Avenue, 11635 Athens, Greece*

[4]*Inamori School of Engineering at the New York State College of Ceramics, Alfred University, 1 Saxon Drive, Alfred, 14802, New York, USA*

[5]*National Institute for Materials Science, 1-1 Namiki, Tsukuba 305-0044, Japan*

**corresponding author:* natalia.wojcik@pg.edu.pl

Keywords: Raman spectroscopy, IR spectroscopy, Beryllium-iron-tellurite glasses, Magnetic properties, Spin-glass

Abstract

In this work, glass-ceramics in the $xBeO–20Fe_2O_3–(80-x)TeO_2$ system with x=0–25 mol% were synthesized by the traditional melt quenching route and studied by inductively coupled plasma optical emission spectroscopy, X-ray diffraction, confocal microscopy, infrared and Raman spectroscopy. BeO addition was found to support the crystallization process of Fe_2O_3 during melting, and an increased BeO content was associated with an increased fraction of the crystalline Fe_2O_3 phase and an increased size of these crystallites. Furthermore, samples doped with BeO exhibit an increasing polymerization of the residual tellurite glass network compared to the undoped sample. The magnetic properties and specific heat of all synthesized materials were measured, and the results show that all studied samples behave as spin-glasses. Also, the Morin transition of hematite was observed at 260 K with intensity depending on the material content in Fe_2O_3 crystalline phase, the formation of which correlates with the amount of added BeO.

1. Introduction

Spin glass materials are of great interest due to their untypical magnetic structure and the presence of phase transition [1]. An interesting spin-glass system is the binary Fe_2O_3-TeO_2 glass which was found to manifest a memory effect below its magnetic transition temperature [2]. Magnetic studies on the same glass system prepared by the sol-gel method show that its magnetic susceptibility follows for low Fe_2O_3 content (up to 10 mol%) the Curie law indicating the paramagnetic nature [3]. It was supposed that in that case iron ions are isolated or participate in dipolar interactions. However, for higher Fe_2O_3 amounts the magnetic properties of Fe_2O_3-TeO_2 glasses are in agreement with the Curie-Weiss law, with the negative paramagnetic Curie temperature being caused by a higher fraction of iron ions participating in superexchange magnetic interactions [3].

Understanding the influence of iron on the nucleation and crystallization kinetics of glasses has been of great interest for the scientific community [4]. Glasses doped with high levels of iron oxide often exhibit a strong tendency towards crystallization, while fully amorphous iron-rich materials can be obtained only after rapid quenching. These materials are also known for their tendency to undergo liquid immiscibility and, consequently, one of the liquid phases is richer in iron and promotes formation of the crystalline phase [5]. Iron

is a transition metal that can co-exist in two oxidation states in any typical glass network, i.e. as Fe^{2+} and Fe^{3+}. The divalent ferrous ion can be best considered to behave as a modifying cation like Ca^{2+}, favoring the high coordination number of six [6]. The trivalent ferric cation can be best described as an intermediate ion, comparable to Al^{3+}, in the fourfold coordination state forming charge deficient $[FeO_4]^-$ tetrahedra which contribute to the glass network, while octahedral coordinated Fe^{3+} has more a network modifier than former role. The ratio of Fe^{2+}/Fe^{3+} in any amorphous structure depends on the chemical composition, the glass basicity [7], as well as the melting conditions such as melting temperature and atmosphere [8, 9]. It was shown that a higher Fe^{2+}/Fe^{3+} ratio lowers the activation energy for the crystallization process, due to a lower viscosity at T_g [4].

TeO_2-containing glasses are widely studied because of their low melting temperature, and their ability to incorporate great amounts of alkali metal ions, transition metal ions and even rare earth ions in the glass network [10-13]. The short-range structure of tellurite glasses involves TeO_4 trigonal bipyramids which convert into TeO_3 trigonal pyramids with non-bridging oxygen atoms as a consequence of doping with, for example, alkali metal oxides [13]. The structure and properties of these glasses are strongly dependent on the nature and quantity of the modifier ions [14]. The influence of Fe_2O_3 addition on the TeO_2-based local glass structure has been previously studied [14-16], however, there is no literature data about the influence of BeO addition on the structure of Fe_2O_3-TeO_2 glass system. The application field of ceramics doped with BeO is quite wide, including for instance high-speed integrated circuits, laser and electronic materials [17]. The beryllium ion is of relatively small size and low weight, and as a high field strength cation, it can behave both as glass former and as modifier ion depending on composition [18, 19]. Unlike other alkaline earths ions, Be^{2+} is always found to be fourfold coordinated to oxygen in crystalline oxides and to form regular BeO_4 tetrahedra in glasses [20, 21].

Due to its rather unique properties, it is of fundamental interest to study the role of Be^{2+} in TeO_2-containing glasses, and this is the primary aim of this work. In this context, the detailed structural analysis is correlated with the magnetic properties of the Fe_2O_3-TeO_2 glass-ceramics doped with different amounts of BeO.

2. Experimental

2.1. Glass preparation

Iron-tellurite glasses doped with beryllium oxide were prepared with the nominal composition $xBeO–20Fe_2O_3–(80-x)TeO_2$ in mol% (designated as xBe), where x=0, 10, 15, 20 and 25 mol%. Appropriate amounts of reagents BeO (99%, Alfa Aesar), Fe_2O_3 (99.9+%, ChemPur GmbH) and TeO_2 (99.99%, ChemPur GmbH) were thoroughly mixed under the protective enclosure of a fume hood. Melting was performed in Al_2O_3 crucibles at 900°C for 60 min, under air atmosphere. Melts were poured on a cold brass plate, and the glasses were annealed for forty-eight hours at a temperature of 370°C under air and cooled to room temperature over 10 hours.

2.2. Glass characterization

2.2.1. X-ray diffraction

Room-temperature powder X-ray diffraction (PXRD) was used to identify the amorphous nature of the samples. This measurement was carried out on a Bruker D2 PHASER diffractometer with CuKα radiation (l = 1.5406 Å) and LynxEye-XE detector. The data were collected from 10 – 90° 2θ over 120 minutes of scan time. The possible errors of XRD results were minimalized by removing the background and are included in the thickness of curves lines.

2.2.2. Chemical composition

The chemical composition of the samples was investigated using an inductively coupled plasma optical emission spectrometer (ICP OES, Aviro 200 Perkin Elmer). Measurements were performed after dissolution of 0.05 g glass powder in 5 ml of aqueous solution of HF acid (40%). All ICP OES values are listed in Table 1. The error margins of ICP-OES analysis were ± 3 % for all elements. The oxygen content was determined from the charge requirements of the analyzed cations. Periodic table mix 1 for ICP measurements (SIGMA ALDRICH, Products number: 92091) contained Be, Fe, Te and Al ions was used as reference standards.

2.2.3. Optical microscopy

The topography of samples was observed by using an Olympus LEXT OLS4000 Confocal Scanning Laser Microscope (CSLM). Color imaging was conducted under white LED light and 3D images were obtained using a 405 nm laser and Photomultiplier Detector. The maximum used objective lens and laser 3D image magnification was 100x, with optical magnification of 2160x. CSLM measurements were obtained from freshly fractured and ethanol cleaned samples as well as on their unpolished surface.

2.2.4. Raman and IR spectroscopy

The structure of glasses was studied by Raman and IR spectroscopy. Raman spectra were measured at the backscattering geometry on a Renishaw inVia Raman Microscope equipped with a 2400 lines/mm diffraction grating, a high-sensitivity Peltier-cooled charge coupled device (CCD), a motorized xyz microscope stage and ×50 magnification lens. All measurements were performed in the range from 200 to 2000 cm^{-1} at room temperature with 2 cm^{-1} resolution. The 514.5 nm line of an Ar ion laser was used for excitation, employing ca. 0.10 $mW/\mu m^2$ at the glass sample to avoid decomposition. Examination of glasses under the Raman microscope after the end of each measurement showed no signs of laser-induced modifications. The sample spot size of the Raman microscope is about 0.5 μm in diameter. Raman spectra were acquired for each glass under VV and VH polarizations, where the first letter indicates the polarization of the exciting laser beam and the second letter the polarization of the scattered light. Unpolarized Raman spectra, VV+VH, were also measured. The estimated error in Raman band position is ± 1 cm^{-1}.

The infrared (IR) spectra were measured on a vacuum Fourier transform spectrometer (Bruker, Vertex 80v) in quasi-specular reflectance mode (11° off-normal). For each spectrum, 400−2000 scans were collected at room temperature with 4 cm^{-1} resolution and averaged for evaluation. Reflectance spectra were measured separately in the far- and mid-IR ranges and then merged to form a continuous spectrum in the range 30−7000 cm^{-1}. Analysis of the reflectance spectra by Kramers−Kronig transformation yielded the absorption coefficient spectra, α(ν) [22]. The estimated error in infrared band position is $\pm$ 2 cm^{-1}.

2.2.5. DTA measurements

Glass transition (T_g), crystallization (T_{cr}) and melting (T_m) temperatures were determined by differential thermal analysis (DTA) with the use of a NETZSCH STA 409PC instrument. The measurements were conducted on powdered samples in Al_2O_3 crucibles, in nitrogen atmosphere and with heating rate of 20 °C min^{-1}. All thermal properties are estimated with precision of ± 2 %.

2.2.6. Magnetic and heat capacity measurements

The dc and ac magnetic measurements were carried out on a Quantum Design Physical Property Measurement System (PPMS) with a vibrating sample magnetometer function (VSM) and the AC Measurement System (ACMS). Data were collected between 1.90 and 300 K in various magnetic fields for powdered samples. Specific heat was measured in zero field using the two-τ time-relaxation method. The sample, pressed into a pellet, was attached to the measuring stage using Apiezon N grease to ensure a good thermal contact.

3. Results and discussion

3.1. Materials synthesis, chemical composition, and morphological characterization

For the synthesized iron-containing glasses, by introducing Fe_2O_3 in a high basicity tellurite glass matrix under air melting in an electric furnace, we would expect that the high oxidation state of iron is the dominant form. This assumption is confirmed by XRD experiments, as presented at the end of this section in more detail.

The melts containing BeO were found to be more homogenous than those without BeO. The content of visible inhomogeneities decreased with increasing Be content as observed on crucible walls after the melting process. Melted materials are non-transparent and black in color. All samples contain inhomogeneities on the surface. Table 1 presents the nominal and the measured chemical compositions by the ICP-OES of the prepared materials. The sample names indicate the nominal BeO content in mol% (x=0, 10, 15, 20 or 25). Comparison of nominal and measured compositions shows a loss of the berryllium, especially for the samples 20Be and 25Be. The quantity of Fe significantly deviates from the starting amount in most of the samples and iron losses were found to increase with Be content. Iron losses can be explained by dilution of the batch composition due to alumina

uptake from the crucible material, as discussed in the next paragraph. For sample 25Be, we observe a significant loss of Te and Be which should be related to evaporation processes during melting. As a consequence, the iron level of this sample appears increased compared to the nominal composition.

All prepared materials contain aluminum, a phenomenon that has been shown for many glasses, as in previous studies using alumina crucibles to prepare phosphate [23, 24] and tellurite glasses [25, 26]. Here, the uptake of Al_2O_3 is the highest for the BeO-free sample (0Be) reaching 5 mol%, while for the BeO-doped samples the amount of Al_2O_3 is lower than 3 mol% (Table 1). Since the Al_2O_3 uptake is low but significant, it will be taken under consideration when discussing the experimental results. It is noted that the opposite correlation was observed for sodium-silicate glasses doped with lithium and beryllium, where the dissolution of Al_2O_3 in the melts was found to be the highest for glasses with the highest BeO quantity [18]. However, the beryllium silicate glasses were prepared from melts at much higher melting temperatures (ca 1450 °C [18]) compared to the 900°C used for the tellurite glasses of the current study. Also, in the silicate system the alumina dissolution correlated with the total concentration of modifier metal oxides M_2O+MO. In addition, charge deficient aluminate tetrahedra enter the silicate network while in tellurite glasses the dissolved aluminates modify the tellurite network. A recent study on niobate dissolution from crucibles materials showed that the dissolution depends on a combination of factors like the melting time, temperature, melt viscosity and basicity [27]. We assume that higher viscosities are related to the Be-rich glasses as the melting temperature increases slightly, and vibrational spectroscopy indicates an increasing tellurite polymerization from 0Be to 20Be (see Sections 3.2, 3.3). In turn, BeO addition does not favor Al_2O_3 dissolution in this system which is free of modifier alkali ions.

Table 1 Glasses ID, nominal and analyzed compositions in the system $xBeO–20Fe_2O_3–(80-x)TeO_2$ and their thermal properties (glass transition temperature, T_g, temperature of crystallization process, T_{cr} and melting point, T_m).

Sample ID	Target composition (in at%)	analyzed glass composition (in at%) ± 3 %	analyzed glass composition (in mol%) ± 3 %	$T_{g\ onset}$ (°C)	$T_{cr\ peak}$ (°C)	T_m (°C)
		$xBeO–20Fe_2O_3–(80-x)TeO_2$				
0Be	$Fe_{11.8}Te_{23.5}O_{64.7}$	$Fe_{9.6}Al_3Te_{23.7}O_{63.8}$	$16Fe_2O_3$-$5Al_2O_3$-$79TeO_2$	420	481	615
10Be	$Be_3Fe_{12.1}Te_{21.2}O_{63.6}$	$Be_{2.7}Fe_{9.3}Al_{1.3}Te_{23.4}O_{63.2}$	8.6BeO-14.8Fe_2O_3-2.1Al_2O_3-74.5TeO_2	421	496	629
15Be	$Be_{4.6}Fe_{12.3}Te_{20}O_{63.1}$	$Be_{4.3}Fe_{11.1}Al_{1.7}Te_{20.7}O_{62.1}$	13.7BeO-17.7Fe_2O_3-2.7Al_2O_3-65.9TeO_2	420	486	637
20Be	$Be_{6.3}Fe_{12.5}Te_{18.8}O_{62.5}$	$Be_{5.5}Fe_{12.5}Al_{1.5}Te_{19}O_{61.5}$	17.5BeO-19.8Fe_2O_3-2.4Al_2O_3-60.3TeO_2	417	478	647
25Be	$Be_{7.9}Fe_{12.7}Te_{17.5}O_{61.9}$	$Be_{6.6}Fe_{15.7}Al_{1.1}Te_{16.3}O_{60.4}$	21.1BeO-25.1Fe_2O_3-1.8Al_2O_3-52.0TeO_2	417	482	649

The topography of the materials was studied on their as-quenched surfaces and on fractures (Figure 1). The micrographs show that all samples are heterogeneous, with the content and size of visible inhomogeneities changing with sample composition. While the surface of the sample 0Be is homogenous and looks like glass, small inhomogeneities are still found on its fracture. After doping with BeO the topography of materials significantly changes. They exhibit small inhomogeneities on their surfaces visible as dots of less than micrometer size, and their content is higher on the as-quenched surfaces than on the fractures. The biggest inhomogeneities are found for samples doped with 20 and 25 mol% BeO as shown in Figure 1. However, as presented for sample 20Be the distribution of bigger inhomogeneities is random and they form clusters, while there are also places exhibiting only small dots (insert of Fig.1). The as-quenched surfaces were more heterogeneous. The differences in materials topography between the as-quenched surfaces and the fractures are a consequence of different cooling rates inside the material and on its surface, differences that occurred during the pouring process. This suggests the decisive influence of the cooling process on sample homogeneity. Additionally, it maybe stated that BeO addition induces the creation of inhomogeneities during the cooling process.

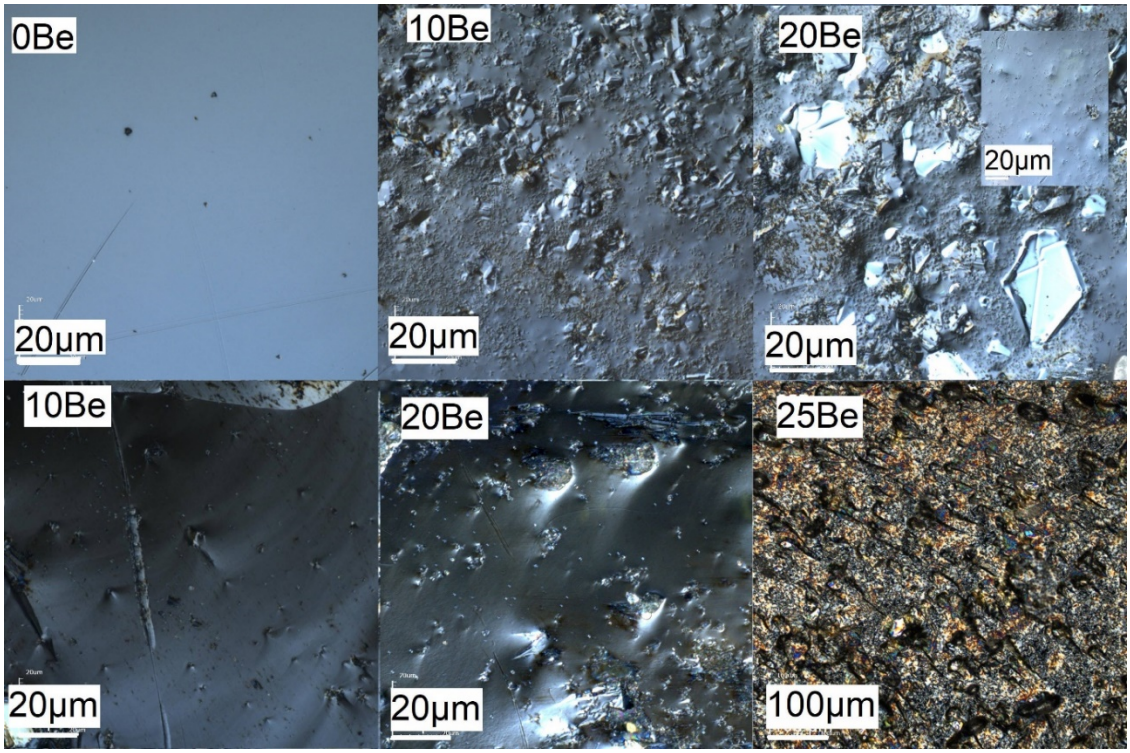

Figure 1. CSLM images of surfaces for samples 0Be, 10Be and 20Be (up), and of fractured samples 10Be, 20Be and 25Be (down).

Figure 2 displays the XRD patterns for all prepared samples. All xBe materials show a typical amorphous halo, which is characteristic for glasses. However, they present in addition some sharp scattering peaks typical of crystalline inclusions, which mostly correspond to Fe_2O_3. All samples exhibit similar results, but with varying degrees of relative intensities and bandwidths of the Fe_2O_3 peaks. The great broadening of most diffraction peaks indicates that the detected crystallites are of less than micrometer size. Especially in the case of samples 0Be and 10Be, the peak maxima for Fe_2O_3 are barely seen. However, the blurring of peaks may also be caused by the amorphous halo coming from the glassy matrix. It can be noticed that the relative intensity of the sharp peaks, and thus the Fe_2O_3 content, increases with increasing BeO content. Furthermore, the XRD patterns for samples 15Be, 20Be and 25Be exhibit a sharp peak at $2\theta \approx 30$ deg which can be correlated with the crystalline phase of Fe_3O_4. As all tested samples have crystalline inclusions, these materials can be referred to as glass-ceramic composites. Moreover, the inhomogeneities found on the samples' surfaces are most probably made of nano- and micrometer sized crystallites of Fe_2O_3 and Fe_3O_4.

For the prepared samples, the proportion of glass and ceramic phase reflects spontaneous crystallization during the initial cooling from the melt. Unlike glass-ceramics that are prepared in a secondary heat treatment process, no specific parameters were controllable. The high content of BeO was found to support the crystallization process. The results of thermal properties (listed in Table 1) showed that the BeO addition does not influence the glass transition and crystallization temperatures, while a slight increase was found for melting point. Further studies might focus on possible post treatments of the samples at elevated temperatures to control the formation of specific crystalline phases.

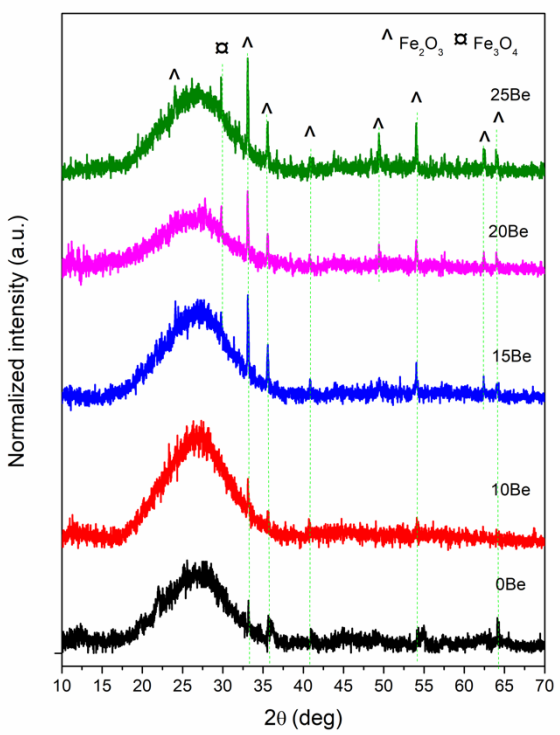

Figure 2. XRD curves of the synthesized samples. For sample compositions corresponding to notations xBe see Table 1.

3.2. *Raman spectroscopy*

Polarized Raman spectra are helpful in assigning bands to symmetric or asymmetric vibrational modes that are Raman active, since the symmetric modes are polarized while the asymmetric ones are depolarized [28]. Figure 3 displays the polarized Raman spectra in parallel (VV) and cross (HV) polarization for samples 0Be (Fig. 3(a)) and 25Be (Fig. 3(b)). As observed in Fig.3, the spectra of both glasses exhibit highly polarized Raman bands at about 440, 660 and 755 cm^{-1} suggesting the association of these bands with symmetric vibrational modes. Indeed, for pure TeO_2 glass [25, 29] and ZnO-containing tellurite glasses [25, 26] the band at 440 cm^{-1} has been attributed to the symmetric stretching-bending mode of Te-O-Te single bridges, v_s(Te-O-Te). The second polarized band at 660-665 cm^{-1} was recently assigned to the symmetric stretching/breathing mode of Te-O_2-Te double bridges, v_s(Te-O_2-Te), connecting TeO_4 trigonal bipyramids (tbp's) with bridging oxygen atoms [29]. The higher frequency envelope at about 755 cm^{-1} develops in tellurite glasses with high content of modifier oxide (for example ZnO) and originates from the symmetric stretching of TeO_3^{2-} trigonal pyramids (tp's) with three terminal oxygen atoms, without excluding some contribution from TeO_{3+1} polyhedra [25, 26]. The notation

TeO_{3+1} indicates a polyhedron where tellurium forms three bonds with one terminal and two bridging oxygen atoms and a fourth weak bond with an oxygen atom at a larger distance (2.2-2.5 Å).

Comparison of the Raman spectrum of the 0Be glass (Fig.3(a)) with that of the undoped (pure) TeO_2 glass [25, 29] shows that the intensity of the 440 cm^{-1} peak is strongly enhanced relative to the 665 cm^{-1} band of the 0Be glass. For Al_2O_3-doped tellurite glasses the enhancement of the 440 cm^{-1} band was attributed to formation of Al-O-Te bridges, the symmetric stretch of which contributes also to the 440 cm^{-1} band envelop. However, the Al_2O_3 content of 0Be glass (5 mol% Al_2O_3) introduced by melting in alumina crucible is not high enough to explain the observed strong enhancement of the 440 cm^{-1} band. This suggests the formation of additional type of bridging bonds between the network units like the Fe-O-Te bridges, because of the relatively high iron content (16 mol% Fe_2O_3) and the same valence of Al and Fe ions (3+). Therefore, the Raman spectrum of glass 0Be indicates that its structure is made mainly of TeO_4 trigonal bipyramids and TeO_3^{2-} trigonal pyramids with the addition of TeO_{3+1} polyhedra. The doping of TeO_2 with 16 mol% Fe_2O_3 and the incorporation of 5 mol% Al_2O_3 through melting provide the required oxygen to cause the depolymerization of the tellurite network through transformation $TeO_4 \rightarrow TeO_{3+1} \rightarrow TeO_3^{2-}$, and the formation of bridges Te-O-Te, Al-O-Te and Fe-O-Te.

The addition of BeO introduces changes in the polarized Raman spectra as seen in Figure 3b, especially for the intense VV spectrum of the sample doped with 25 mol% BeO. In particular, the band at ~660 cm^{-1} gains relative intensity in comparison to the 755 cm^{-1} band, indicating an increased population of TeO_4 units over TeO_3^{2-} and TeO_{3+1} units. This manifests a lower modification of the glassy tellurite matrix of the 25Be glass-ceramic relative to the 0Be glass, despite the fact that 25Be has a larger total modifier content than 0Be (Table 1). In addition to these changes, the Raman spectrum of sample 25Be shows two weak and sharp features at 227 and 293 cm^{-1} in both VV and HV polarizations. These indicate the formation of a crystalline Fe_2O_3 phase [30], in accordance with the XRD results. The partial crystallization of the 25Be sample during the melting process removes Fe_2O_3 from the glassy matrix and, thus, reduces the amount of Fe_2O_3 available for modification of the tellurite matrix as manifested by the enhancement of the ~660 cm^{-1} band. In addition, a partial removal of Fe_2O_3 from the tellurite matrix would decrease the number of Fe-O-Te bridges and causes a decrease in relative intensity of the 440 cm^{-1} band (Fig. 3b).

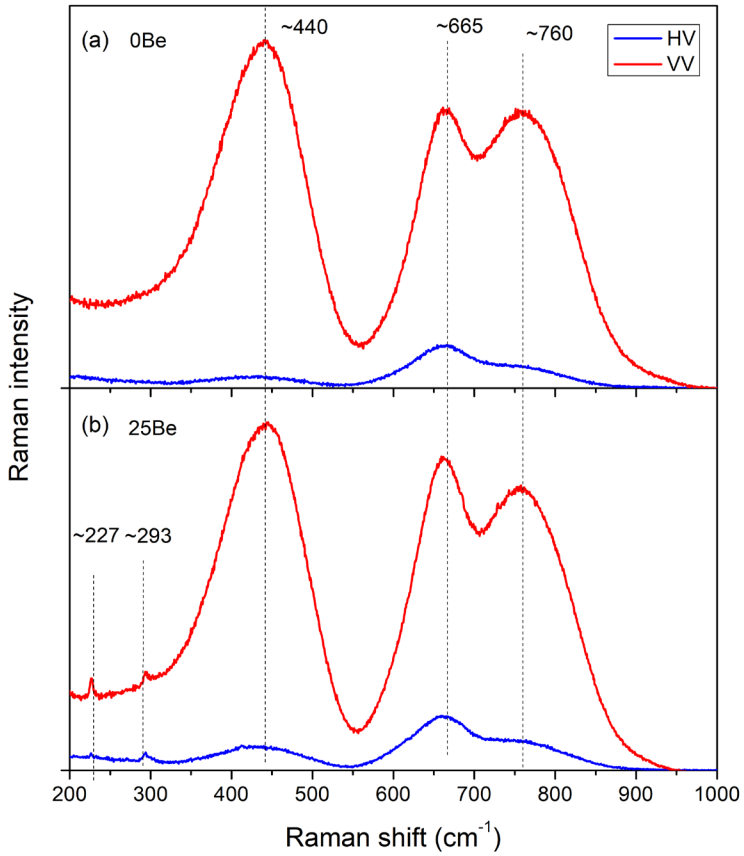

Figure 3. Polarized Raman spectra in parallel (VV, red) and cross (HV, blue) polarization for samples: (a) 0Be and (b) 25 Be.

To illustrate the influence of BeO doping on the tellurite glass network in the entire composition range, and allow observing spectral changes and corresponding structural modifications, the polarized VV spectra were scaled on the strongest band at 440 cm^{-1} and are depicted in Fig. 4. It is found that the band at 660 cm^{-1}, characteristic of connected TeO_4 trigonal bipyramids, increases in intensity relative to those at 440 and 760 cm^{-1}. This shows again that addition of BeO causes the decrease of tellurite network modification, i.e. increased content of TeO_4 units relative to the TeO_{3+1} and TeO_3^{2-} modified tellurite polyhedra. We pay special attention to glass-ceramic 10Be because the intensity of its 660 cm^{-1} band is not between those of the 0Be and 15Be samples (Fig. 4). Instead, the 10Be intensity appears higher than for 15Be and, thus, suggests a lower tellurite modification in 10Be. This Raman result is consistent with chemical analysis giving the

lowest Fe and Al content in 10Be compared to all other tested samples (Table 1). In agreement with these observations is the finding that the content and size of the Fe_2O_3 crystalline phase is among all BeO-doped samples the lowest in sample 10Be (Fig. 2). Most probably, only part of the Fe ion concentration creates crystallites of the Fe_2O_3 phase, which are distributed unevenly in the residual glass matrix. The rest of the Fe ions, together with Al and Be ions play the role of tellurite matrix modifiers. The Raman spectra suggest that the combined influence of all oxide modifiers is the lowest for sample 10Be and, therefore, the polymerization of its tellurite glass network is higher than for the 15Be and 0Be samples.

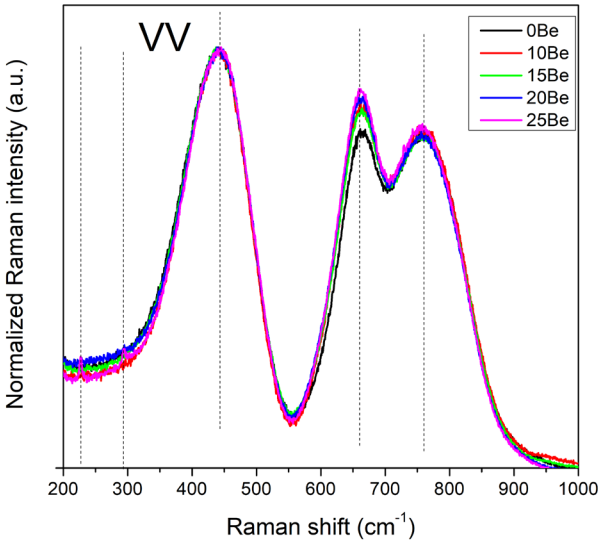

Figure 4. Comparison of the VV polarized Raman spectra for all glass-ceramics xBe, after normalization on the strongest band envelop at 440 cm^{-1}.

To ensure that the trends discussed above do not result exclusively from the VV polarized spectra, we considered in addition the unpolarized (VV+VH) Raman spectra for all samples as shown in Figure 5a. The Raman spectra were scaled again on the strongest band at 440 cm^{-1} to facilitate comparison. One clearly visible difference in the Raman spectra concerns the middle frequency band at ~660 cm^{-1}, which is shown in Figure 5b in larger frequency magnification. It is noticed that the position of this band moves from higher (665 cm^{-1}, 0Be) to lower frequency (660 cm^{-1}, 25Be) and its intensity increases with the progressive addition of BeO. Considering that the strongest Raman band of pure TeO_2 glass is measured at 660 cm^{-1} [25, 29], this result suggests again the increase in the degree of tellurite polymerization from 0Be to 25Be. This can be due to the fact that the added

BeO highly influences the content of crystalline Fe_2O_3 phase which crystallizes during the melting/cooling process. It was found that the higher the BeO amount the higher is the quantity of the crystalline Fe_2O_3 phase and the size of the crystallites increases. As a consequence, the content of residual Fe ions in the glass matrix is lower for samples highly doped with BeO. Therefore, the tellurite glass matrix becomes slightly poorer in total modifier ions, i.e. in Fe, Al and Be ions which are available to destruct the TeO_4 trigonal bipyramids. Consequently, the Raman spectra of samples doped with BeO show higher polymerization of the tellurite glass network than before doping (0Be).

The presence of a crystalline Fe_2O_3 phase was confirmed by XRD and for samples 20Be and 25Be is also indicated by sharp peaks at 227 and 293 cm^{-1} in the polarized and unpolarized Raman spectra. It is of interest to note the much smaller contribution of the crystalline Fe_2O_3 phase signatures in the Raman spectra (Figs. 4 and 5) relative to the strong evidence in the XRD patterns (Fig. 2). The lack of these peaks in the Raman spectra of other samples may suggest that the size and amount of Fe_2O_3 crystallites is too small to be detected by Raman spectroscopy. An additional reason for the relatively weak Raman contribution of the Fe_2O_3 phase within the tellurite matrix should be the larger polarizability of Te-O bonds compared to Fe-O bonds. This is because of the higher polarizability, α, of the Te^{4+} ion compared to Fe^{3+}, with $\alpha_{Te^{4+}}$=1.595 $Å^3$ and $\alpha_{Fe^{3+}}$=0.437 $Å^3$ [31]. Since the Raman intensity of a vibrational mode is proportional to the square of the polarizability derivative with respect to the normal coordinate of the mode, the Raman scattering cross section of Te-O related vibrations should be significantly larger compared to Fe-O related modes. Consequently, even a considerable number of Fe-O bonds in a tellurite matrix are expected to show relatively weak Raman signals. Even weaker contributions are expected for the Be-O and Al-O related vibrations in the tellurite matrix, since $\alpha_{Be^{2+}}$=0.008 $Å^3$ and $\alpha_{Al^{3+}}$=0.054 $Å^3$ [30] and, thus, they will be completely overmasked by the tellurite response.

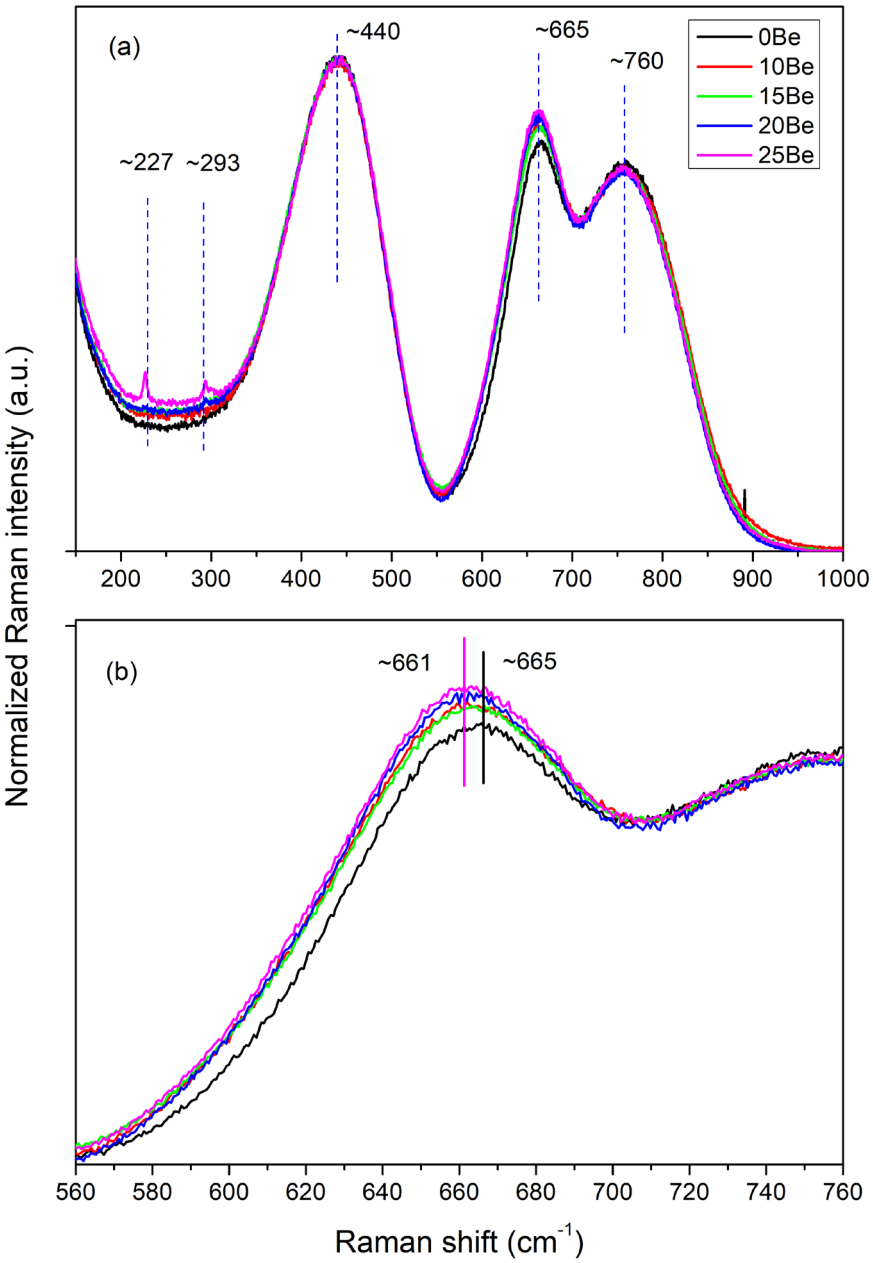

Figure 5. (a) Unpolarized (VV+VH) Raman spectra of all glass-ceramics scaled on the 440 cm^{-1} band. (b) Magnification of the frequency range of the band at ~660 cm^{-1} for all glass-ceramics after normalization to the intensity of the low frequency envelop at 440 cm^{-1}.

3.3. *IR spectroscopy*

A complementary method for probing the structure of the synthesized glass-ceramics is IR spectroscopy, where changes in the dipole moment of the vibrating structural units determine their infrared activity. The infrared spectra of all glass-ceramics composites are shown in Figure 6. While the VV Raman spectra are dominated by the symmetric stretching

and bending vibrations of tellurite species, the corresponding asymmetric vibrational modes are strongly active in the infrared. Thus, the broad and asymmetric IR envelop observed at high frequencies should result from the convolution of the asymmetric stretching modes of TeO_3^{2-}, TeO_{3+1} and TeO_4 units [26]. Starting with the 0Be glass, the TeO_3^{2-} and TeO_{3+1} units should contribute to the ca. 685 cm^{-1} peak while the shoulder at ca. 650 cm^{-1} manifests the presence of TeO_4 units, considering that pure TeO_2 glass gives it strongest infrared absorption at 655 cm^{-1} [25, 29]. As the BeO content increases, the 650 cm^{-1} shoulder gains relative intensity and the entire high-frequency envelop downshifts from 685 cm^{-1} (0Be) to 675 cm^{-1} (20Be). This is a clear manifestation of an increasing tellurite polymerization from 0Be to 20Be as found also by Raman spectroscopy. In terms of its high-frequency envelop peaking at 675 cm^{-1}, sample 10Be appears more modified than 15Be (685 cm^{-1}) and similar to 20Be, in agreement with the Raman spectroscopic results.

The IR spectrum of the 25Be material appears as outlier when compared to the rest of the spectra, since it shows considerable broadening of the strongest IR band at high-frequencies and upshifting of its main peak maximum to about 730 cm^{-1} (Fig. 6). This suggests the formation of new types of structural units in addition to the tellurite species already discussed. The high BeO content of this glass (20 mol%) may lead to formation of $[BeO_{4/2}]^{2-}$ tetrahedral units, with Be-O stretching active at about 750 cm^{-1} [18]. Additional broadening at high frequencies may result from weaker contributions of Al-O stretching in $[AlO_{4/2}]^{-}$ tetrahedra which absorb above 700 cm^{-1} [18].

The 25Be sample has also the highest Fe_2O_3 concentration (25 mol%) and the largest Fe_2O_3 crystalline content according to XRD (Fig. 2). Infrared evidence for the presence of a crystalline Fe_2O_3 phase is provided by the relatively sharp features at 730, 490 and 350 cm^{-1} [30, 32, 33], while additional absorption of FeO_4 units at 570-600 cm^{-1} [14] would overlap with the tellurite activity in the same range. Additionally, the Fe_2O_3 dissolved in the glassy matrix and acting as modifier of the tellurite network would probably form FeO_6 octahedral units which are expected to absorb in the 400-500 cm^{-1} range [14]. While the broad 350-500 cm^{-1} envelop originates mainly from stretching-bending vibrations of O-Te-O and Te-O-Te bonding in various tellurite configurations [29], weak absorption seen at about 400 cm^{-1} may be also related to FeO_6 units.

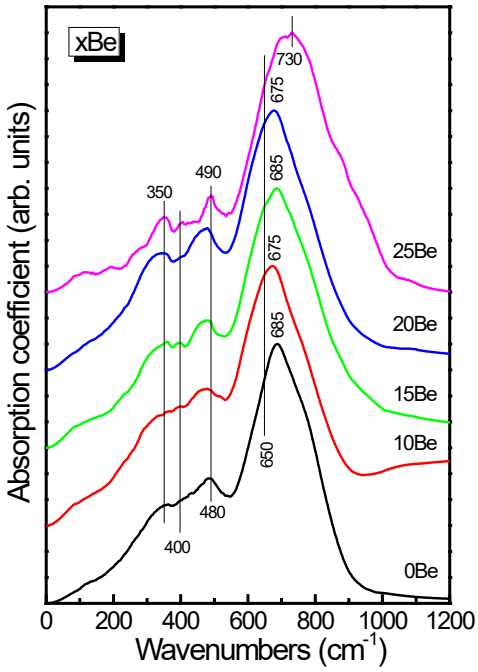

Figure 6. Absorption coefficient spectra of glass-ceramic xBe samples, normalized on their highest intensity band.

In comparison to our findings, we note that a study of glasses xFe_2O_3–$(1-x)TeO_2$, which were melted in alumina crucible with x=0.05 to x=0.20 and studied by X-ray photoelectron spectroscopy, concluded that the Te atoms exist only in TeO_4 trigonal bipyramids [15]. This interesting finding is in disagreement with our results for the 0Be glass which has the closest composition to the x=0.20 glass of [15]. Both IR and Raman spectroscopy of 0Be showed the coexistence of TeO_4 with TeO_3^{2-} and TeO_{3+1} units. An additional finding of work [15] was the presence of oxygen atoms in Te–O–Te, Te–O–Fe, and Fe–O–Fe bonding configurations where they have similar binding energies, and with iron ions existing predominantly in the Fe^{3+} state. This is in accordance with the crystalline phase detected in our xBe samples.

3.4. Magnetic properties

Magnetic measurements were carried out for all samples. At low temperatures, the transition related to the occurrence of a spin-glass phase was observed. Figure 7 presents results obtained for the 25Be sample measured below 15 K. The inset of Figure 7(a) shows the temperature dependent real part of the ac magnetization (H_{ac}=10 Oe) for frequencies f = 125, 539, 2321 and 10000 Hz. The maximum in the real and imaginary (not shown

here) part of the magnetization increases and shifts towards lower temperature as the frequency of the excitation field is decreased. The frequency dependence of both components is a characteristic feature of spin-glass materials [34-37] and, hence, suggests the formation of a spin-glass state in the sample.

A widely accepted criterion for distinguishing different spin-glass systems is to compare a relative shift in freezing temperature (T_f) per decade of frequency [35, 38]. For isolated clusters (superparamagnets), it is of the order of 0.3 [39], whilst for spin–glass systems the quantity varies in the range of 0.004−0.018 [39]. Using the equation $\delta T_f = \frac{\Delta T_f}{T_f \Delta(log_{10} f)}$, for the 25Be sample we found $\delta T_f = 0.020$, which suggests the spin-glass state at low temperatures. A value of relative shift, estimated for all samples, is very nearly the same. In the next step, we have used the simple Vogel-Fulcher equation: $T_f = T_0 - \frac{E_a}{k_B} \frac{1}{\ln(\tau_0 f)}$, where T_0, E_a and τ_0 are the Vogel – Fulcher temperature, with E_a and τ_0 being the activation energy and the intrinsic relaxation time, respectively. Figure 8a depicts a plot of the temperature freezing (T_f) versus $1/\ln(\tau_0 f)$, where τ_0 = 10^{-13}s, typical for the spin-glass systems [37, 39-41]. Data were fitted by the above formula and the fit, shown by the red solid line, gave T_0 = $4.34(6)\ K$ and E_a/k_B = $30(1)\ K$. Therefore, an estimated activation energy is E_a ~ $5.05\ k_B T_f$. The calculated value is comparable with those obtained for other spin-glass compounds (e.g. Fe_2TiO_5 $\left(3.4\ k_B T_f\right)$[42]).

Figure 7b shows the dc magnetization in field cooling (FC) and in zero-field cooling (ZFC) modes, taken as a function of temperature in a constant magnetic field of 1000 Oe. The FC curve increases monotonically with decreasing temperature, whilst the ZFC line exhibits a maximum. Below a certain temperature (T_f=4.45 K), ZFC and FC magnetization curves manifest a significant irreversibility, this feature being attributed to the formation of a glassy state. Figure 7c shows the temperature dependence of the zero-field specific heat C_p/T from 1.95 to 15 K. Around the transition temperature (T_f), one can observe a weak anomaly (weak increase of Cp/T) which is consistent with a spin-glass state scenario. This demonstrates clearly that the maximum in the ZFC magnetization is not related to a long-range ordering of the magnetic moments [43-45]. Similar behavior is observed for all tested samples.

Analogous magnetic behavior was observed for the $20Fe_2O_3$-$80TeO_2$ glass which is free of BeO and Al_2O_3. It was found that this glass converts into a spin glass phase at a

very low temperature. The mechanism of magnetic transition presumably depends on the specific glass, i.e. the concentration of magnetic ions and the preparation process of the glass [2].

The current results are in accord with the previous findings that all samples exhibit similar magnetic properties in the low temperature range, which suggest that they are spin-glasses. However, they contain different amounts of the crystalline phase Fe_2O_3 and Fe ions which determine the magnetic properties. This may suggest that in all samples, the residual of Fe ions are randomly distributed in the glass matrix. Moreover, there is no detectable influence of Be addition on the low temperature magnetic properties of the studied Fe-Te-Al-O glass-ceramic composites.

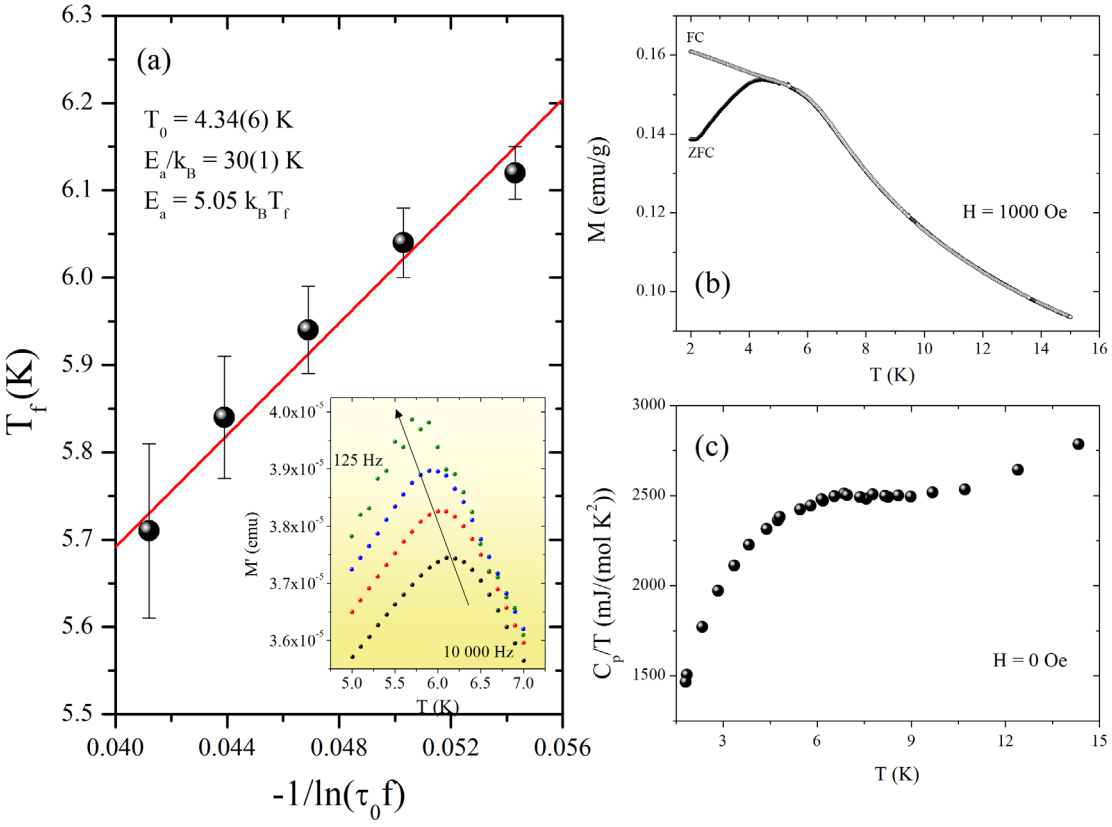

Figure 7. (a) The freezing temperature (T_f) versus $1/\ln(\tau_0 f)$, where τ_0 = 10^{-13}s, measured below 15 K. The red line is the fit of the Vogel-Fulcher equation to the data. The inset of figure (a) indicates the temperature dependent real part of the ac magnetization (H_{ac} = 10 Oe) for frequencies f = 125, 539, 2321 and 10000 Hz. **(b)** The dc magnetization M(T) in field cooling (FC) and in zero-field cooling (ZFC) modes, taken as a function of temperature in a constant magnetic field of 1000 Oe. **(c)** The temperature dependence of the zero-field specific heat C_p/T from 1.95 to 15 K. All presented results are for sample 25Be.

However, the influence of Be addition was observed at higher temperatures. Figure 8 presents the magnetization of all samples as a function of temperature in the range 220–320 K under an applied magnetic field of 1000 Oe. The high-temperature anomaly is assigned to crystalline Fe_2O_3 and is known as Morin transition (or spin-flop transition). This magnetic phase transition in hematite is observed at ~250 K [46]. Below this temperature, the structure of hematite is antiferromagnetic and it changes to weakly ferromagnetic on heating through 250 K. The Morin transition is most pronounced for sample 25Be, while the lack of an anomaly is observed for sample 0Be. These findings may be correlated with the content of the Fe_2O_3 crystalline phase, which was found by XRD to be the highest for sample 25Be and almost imperceptible for samples 0Be and 10Be (see Fig. 2).

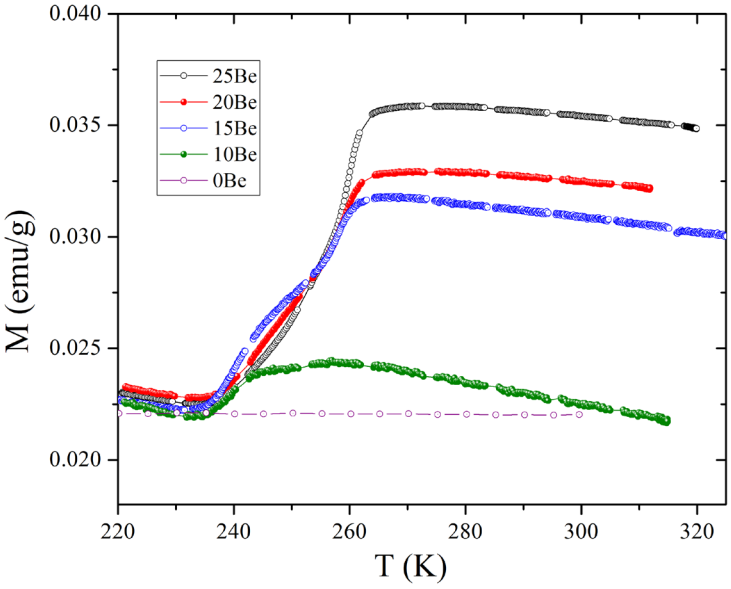

Figure 8. Dependence of magnetization on temperature and composition under an applied magnetic field of 1000 Oe.

4. Conclusions

BeO-Fe_2O_3-Al_2O_3-TeO_2 glass-ceramic composites doped with different content of BeO were prepared. The BeO doping did not favor Al_2O_3 dissolution from the crucible material but induced the formation of inhomogeneities. The observed inhomogeneities were correlated with crystallites of Fe_2O_3 and Fe_3O_4. The structure of the BeO-free glass was found to consist mainly of TeO_4 trigonal bipyramids and TeO_3^{2-} trigonal pyramids with the addition of TeO_{3+1} polyhedra. The addition of Fe_2O_3 and the incorporation of Al_2O_3 through melting caused the depolymerization of the tellurite network and the formation of

various oxygen linkages Te-O-Te, Al-O-Te and Fe-O-Te. However, doping with BeO caused the increase of tellurite network polymerization. Some of the Fe ions create crystallites of the Fe_2O_3 phase, which are unevenly distributed in the residual glass matrix. The residual Fe ions, together with Al and Be ions take on the role of tellurite matrix modifiers.

Magnetic measurements indicate that all samples exhibit similar magnetic properties in the low temperature range, which suggests that they are spin-glasses. No detectable influence of Be addition on the low temperature magnetic properties of Fe-Te-Al-O samples was noticed. However, in the high temperature range, a magnetic anomaly was detected and assigned to Morin transition, typical for hematite. The Morin transition was most pronounced for the sample doped with the highest amount of BeO (25 mol%), while the lack of an anomaly was observed for the BeO-free sample.

Acknowledgements

SA and NW acknowledge the financial support from the Crafoord Foundation (Grant No: 20160900) and Vinnova (Grant No. 2015-04809). NST and EIK acknowledge support by the project "National Infrastructure in Nanotechnology, Advanced Materials and Micro-/Nanoelectronics" (MIS 5002772), funded by the Operational Programme "Competitiveness, Entrepreneurship and Innovation" (NSRF 2014-2020) and co-financed by Greece and the European Union (European Regional Development Fund).

References

[1] V. Cannella, J.A. Mydosh, Magnetic ordering in gold-iron alloys, Physical Review B, 6 (1972) 4220-4237.

[2] H. Akamatsu, K. Tanaka, K. Fujita, Spin dynamics in Fe_2O_3-TeO_2 glass: experimental evidence for an amorphous oxide spin glass, Physical Review B, 74 (2006).

[3] A. Dehelean, E. Culea, Magnetic studies of TeO_2 - Fe_2O_3 glass systems obtained by the sol - gel method, Journal of Physics: Conference Series, 182 (2009).

[4] Y. Shaharyar, J.Y. Cheng, E. Han, A. Maron, J. Weaver, J. Marcial, J.S. McCloy, A. Goel, Elucidating the effect of iron speciation (Fe^{2+}/Fe^{3+}) on crystallization kinetics of

sodium aluminosilicate glasses, Journal of the American Ceramic Society, 99 (2016) 2306-2315.
[5] A. Karamanov, P. Pisciella, C. Cantalini, M. Pelino, Influence of Fe^{3+}/Fe^{2+} Ratio on the crystallization of iron-rich glasses made with industrial wastes, Journal of the American Ceramic Society, 83 (2000) 3153-3157.
[6] T.T. Volotinen, J.M. Parker, P.A. Bingham, Concentrations and site partitioning of Fe^{2+} and Fe^{3+} ions in a soda–lime–silica glass obtained by optical absorbance spectroscopy, Phys. Chem. Glasses - Eur. J. Glass Sci. Technol. B, 49 (2008) 258-270.
[7] J.A. Duffy, Redox equilibria in glass, Journal of Non-Crystalline Solids, 196 (1996) 45-50.
[8] A. Paul, Oxidation — reduction equilibrium in glass forming melts, in: R.A. Levy, R. Hasegawa (Eds.) Amorphous Magnetism II, Springer US, Boston, MA, 1977, pp. 597-611.
[9] P. Stabile, G. Giuli, M.R. Cicconi, E. Paris, A. Trapananti, H. Behrens, The effect of oxygen fugacity and Na/(Na+K) ratio on iron speciation in pantelleritic glasses, Journal of Non-Crystalline Solids, 478 (2017).
[10] Sanjay, N. Kishore, M.S. Sheoran, S. Devi, Study of boro-tellurite glasses doped with neodymium oxide, AIP Conference Proceedings, 1953 (2018) 090049.
[11] G.D. Khattak, A. Mekki, L.E. Wenger, Local structure and redox state of copper in tellurite glasses, Journal of Non-Crystalline Solids, 337 (2004) 174-181.
[12] R.A. El-Mallawany, G.A. Saunders, Elastic properties of binary, ternary and quaternary rare earth tellurite glasses, J Mater Sci Lett, 7 (1988) 870-874.
[13] A. Mekki, G.D. Khattak, L.E. Wenger, Structural and magnetic properties of MoO3–TeO2 glasses, Journal of Non-Crystalline Solids, 351 (2005) 2493-2500.
[14] S. Rada, A. Dehelean, E. Culea, FTIR, Raman, and UV-Vis spectroscopic and DFT investigations of the structure of iron–lead–tellurate glasses, Journal of molecular modeling, 17 (2010) 2103-2111.
[15] A. Mekki, G.D. Khattak, L.E. Wenger, Structural and magnetic investigations of Fe_2O_3–TeO_2 glasses, Journal of Non-Crystalline Solids, 352 (2006) 3326-3331.
[16] I. Shaltout, Crystallization kinetics and structure of (TeO_2-TiO_2-Fe_2O_3) glasses, Journal of Materials Science, 35 (2000) 323-329.
[17] T.P. Ellen, M. Costa, 14.08 - Carcinogenic inorganic chemicals* A2 - McQueen, Charlene A, in: Comprehensive toxicology (Second Edition), Elsevier, Oxford, 2010, pp. 139-160.

[18] N.A. Wójcik, S. Ali, D. Möncke, N.S. Tagiara, E.I. Kamitsos, H. Segawa, M. Eriksson, B. Jonson, The influence of Be addition on the structure and thermal properties of alkali-silicate glasses, Journal of Non-Crystalline Solids, 521 (2019) 119532.
[19] N.A. Wójcik, P. Kupracz, R.J. Barczyński, B. Jonson, S. Ali, Ion conduction in beryllium-alumino-silicate glasses doped with sodium or sodium and lithium ions, Solid State Ionics, 341 (2019) 115055.
[20] S. Sen, P. Yu, Observation of a stuffed unmodified network in beryllium silicate glasses with multinuclear NMR spectroscopy, Physical Review B, 72 (2005) 132203.
[21] D. Möncke, S. Ali, B. Jonson, E.I. Kamitsos, Anion polarizabilities in oxynitride glasses. Establishing a common optical basicity scale, Physical Chemistry Chemical Physics, 22 (2020) 9543-9560.
[22] E.I. Kamitsos, Infrared spectroscopy of glasses, in: M. Affatigato (Ed.) Modern glass characterization, John Wiley & Sons, Inc., 2015, pp. 32-73.
[23] I. Konidakis, C.P.E. Varsamis, E.I. Kamitsos, Effect of synthesis method on the structure and properties of $AgPO_3$-based glasses, Journal of Non-Crystalline Solids, 357 (2011) 2684-2689.
[24] D. Palles, I. Konidakis, C.P.E. Varsamis, E.I. Kamitsos, Vibrational spectroscopic and bond valence study of structure and bonding in Al_2O_3-containing AgI-$AgPO_3$ glasses, RSC Advances, 6 (2016) 16697-16710.
[25] N.S. Tagiara, D. Palles, E.D. Simandiras, V. Psycharis, A. Kyritsis, E.I. Kamitsos, Synthesis, thermal and structural properties of pure TeO_2 glass and zinc-tellurite glasses, Journal of Non-Crystalline Solids, 457 (2017) 116-125.
[26] N.S. Tagiara, E. Moayedi, A. Kyritsis, L. Wondraczek, E.I. Kamitsos, Short-range structure, thermal and elastic properties of binary and ternary tellurite glasses, The Journal of Physical Chemistry B, 123 (2019) 7905-7918.
[27] N.A. Wójcik, S. Ali, E.I. Kamitsos, D. Möncke, Niobate in silicate and phosphate glasses – crucible dissolution as function of glass basicity, will be submitted, (2021).
[28] I. Efthimiopoulos, D. Palles, S. Richter, U. Hoppe, D. Möncke, L. Wondraczek, S. Nolte, E.I. Kamitsos, Femtosecond laser-induced transformations in ultra-low expansion glass: Microstructure and local density variations by vibrational spectroscopy, J Appl Phys, 123 (2018) 233105.
[29] A.G. Papadopoulos, N.S. Tagiara, E.D. Simandiras, E.I. Kamitsos, On the absence of doubly bonded Te═O groups in TeO_2 glass, The Journal of Physical Chemistry B, 124 (2020) 5746-5753.

[30] S.-H. Shim, T. Duffy, Raman spectroscopy of Fe_2O_3 to 62 GPa, American Mineralogist, 87 (2002).
[31] V. Dimitrov, T. Komatsu, An interpretation of optical properties of oxides and oxide glasses in terms of the electronic ion polarizability and average single bond strength, Journal of the University of Chemical Technology and Metallurgy, 45 (2010) 219-250.
[32] W.A. Kaczmarek, I. Onyskiewicz, B. Ninham, Structural and magnetic characteristic of novel method of $Fe_2O_3 \Rightarrow Fe_3O_4$ reduction by magnetomechanical activation, Magnetics, IEEE Transactions on, 30 (1994) 4725-4727.
[33] I. Jacyna-Onyszkiewicz, M. Grunwald-Wyspianska, W. Kaczmarek, A., IR Studies of the phase transformation of $Fe_2O_3 \rightarrow Fe_3O_4$ by magnetomechanical activation, J. Phys. IV France, 07 (1997) C1-615-C611-616.
[34] V.K. Anand, D.T. Adroja, A.D. Hillier, Ferromagnetic cluster spin-glass behavior in $PrRhSn_3$, Physical Review B, 85 (2012) 014418.
[35] T. Mori, H. Mamiya, Dynamical properties of a crystalline rare-earth boron cluster spin-glass system, Physical Review B, 68 (2003) 214422.
[36] S. Mukherjee, A.K. Pal, S. Bhattacharya, J. Raittila, Magnetism of Mn_2O_3 nanocrystals dispersed in a silica matrix: Size effects and phase transformations, Physical Review B, 74 (2006) 104413.
[37] J.L. Tholence, On the frequency dependence of the transition temperature in spin glasses, Solid State Communications, 35 (1980) 113-117.
[38] C.A. Cardoso, F.M. Araujo-Moreira, V.P.S. Awana, E. Takayama-Muromachi, O.F. de Lima, H. Yamauchi, M. Karppinen, Spin glass behavior in $RuSr_2Gd_{1.5}Ce_{0.5}Cu_2O_{10-\delta}$, Physical Review B, 67 (2003) 020407.
[39] J.A. Mydosh, Spin glasses: an experimental introduction, Taylor and Francis, London, 1993.
[40] K. Górnicka, K.K. Kolincio, T. Klimczuk, Spin-glass behavior in a binary Pr_3Ir intermetallic compound, Intermetallics, 100 (2018) 63-69.
[41] J. Prejean, J., Time and temperature evolution of the saturated thermoremanent magnetization of a spin glass, J. Phys. Colloques, 39 (1978) C6-907-C906-909.
[42] J.L. Tholence, Y. Yeshurun, J.K. Kjems, B. Wanklyn, Spin dynamics and low temperature properties of the anisotropic spin glass Fe_2TiO_5, Journal of Magnetism and Magnetic Materials, 54-57 (1986) 203-204.

[43] D. Li, Y. Homma, F. Honda, T. Yamamura, D. Aoki, Low temperature spin-glass behavior in nonmagnetic atom disorder compound Pr_2CuIn_3, Physics Procedia, 75 (2015) 703-710.
[44] T. Mori, A. Leithe-Jasper, Spin glass behavior in rhombohedral B_{12} cluster compounds, Physical Review B, 66 (2002) 214419.
[45] D.X. Li, S. Nimori, Y. Shiokawa, Y. Haga, E. Yamamoto, Y. Onuki, Ferromagnetic cluster glass behavior in U_2IrSi_3, Physical Review B, 68 (2003) 172405.
[46] F.J. Morin, Magnetic susceptibility of Fe_2O_3 and Fe_2O_3 with added titanium, Physical Review, 78 (1950) 819-820.